

# Differential contribution of excitatory and inhibitory neurons in shaping neurovascular coupling in different epileptic neural states

Journal of Cerebral Blood Flow & Metabolism  
2021, Vol. 41(5) 1145–1161  
© The Author(s) 2020



Article reuse guidelines:  
sagepub.com/journals-permissions  
DOI: 10.1177/0271678X20934071  
journals.sagepub.com/home/jcbfm



Hyun-Kyoung Lim<sup>1,2</sup> , Nayeon You<sup>1,3</sup>, Sungjun Bae<sup>1,3</sup>,  
Bok-Man Kang<sup>1,3</sup>, Young-Min Shon<sup>4</sup>, Seong-Gi Kim<sup>1,3,6</sup> and  
Minah Suh<sup>1,3,5,6</sup>

## Abstract

Understanding the neurovascular coupling (NVC) underlying hemodynamic changes in epilepsy is crucial to properly interpreting functional brain imaging signals associated with epileptic events. However, how excitatory and inhibitory neurons affect vascular responses in different epileptic states remains unknown. We conducted real-time *in vivo* measurements of cerebral blood flow (CBF), vessel diameter, and excitatory and inhibitory neuronal calcium signals during recurrent focal seizures. During preictal states, decreases in CBF and arteriole diameter were closely related to decreased  $\gamma$ -band local field potential (LFP) power, which was linked to relatively elevated excitatory and reduced inhibitory neuronal activity levels. Notably, this preictal condition was followed by a strengthened ictal event. In particular, the preictal inhibitory activity level was positively correlated with coherent oscillating activity specific to inhibitory neurons. In contrast, ictal states were characterized by elevated synchrony in excitatory neurons. Given these findings, we suggest that excitatory and inhibitory neurons differentially contribute to shaping the ictal and preictal neural states, respectively. Moreover, the preictal vascular activity, alongside with the  $\gamma$ -band, may reflect the relative levels of excitatory and inhibitory neuronal activity, and upcoming ictal activity. Our findings provide useful insights into how perfusion signals of different epileptic states are related in terms of NVC.

## Keywords

Epilepsy, neurovascular coupling, *in vivo* two-photon imaging, calcium imaging, excitatory neuron, inhibitory neuron, cerebral blood flow

Received 3 March 2020; Revised 14 May 2020; Accepted 17 May 2020

## Introduction

Epileptic events represent pathological alterations in neural networks that involve sporadic and recurrent episodes of excessive brain activity. To delineate an epileptogenic zone, perfusion-based imaging methods such as single-photon emission computed tomography (SPECT), positron emission tomography (PET), and functional magnetic resonance imaging (fMRI) have been widely utilized owing to their noninvasiveness and the accessibility of a wide range of brain regions. Abnormal perfusion or metabolic changes, such as ictal hyperperfusion<sup>1–8</sup> and interictal or postictal hypoperfusion,<sup>5,6,9–14</sup> in specific brain areas are generally used

<sup>1</sup>Center for Neuroscience Imaging Research (CNIR), Institute for Basic Science (IBS), Suwon, South Korea

<sup>2</sup>Department of Biological Sciences, Sungkyunkwan University, Suwon, South Korea

<sup>3</sup>Department of Biomedical Engineering, Sungkyunkwan University, Suwon, South Korea

<sup>4</sup>Department of Neurology, Samsung Medical Center, Sungkyunkwan University School of Medicine, Seoul, South Korea

<sup>5</sup>Biomedical Institute for Convergence at SKKU (BICS), Sungkyunkwan University, Suwon, South Korea

<sup>6</sup>Samsung Advanced Institute for Health Sciences & Technology (SAIHST), Sungkyunkwan University, Suwon, South Korea

## Corresponding author:

Minah Suh, Department of Biomedical Engineering, Sungkyunkwan University, Suwon 16419, South Korea.

Email: minahsuh@skku.edu

to characterize potential biomarkers of epileptogenic foci. Spatial brain mapping of differences in perfusion signals between different epileptic states, e.g. interictal and ictal states, has also been used.<sup>4,15–18</sup> Thus, understanding the neurovascular coupling (NVC) that underlie blood flow changes in different epileptic states is fundamental.

Ictal states are well known for neuronal hyperactivity in both excitatory and inhibitory neurons.<sup>19–24</sup> Animal studies related to NVC in epilepsy have shown that ictal events evoke drastic increases in vessel diameter<sup>25–27</sup> and cerebral blood flow (CBF)<sup>28,29</sup> due to high metabolic demand caused by intense neuronal activity.<sup>26,29,30</sup> On the other hand, interictal or preictal states preceding ictal onset are characterized by GABAergic interneuronal activity,<sup>21,31–33</sup> which is considered to play a crucial role in shaping the transition to ictal states.<sup>21,23,24,34,35</sup> Considering that GABAergic interneuronal activity is known to be an important contributor to the regulation of blood flow,<sup>36–41</sup> the distinct inhibitory neuronal activities that occur during interictal or preictal states can potentially result in CBF changes. Thus, neurovascular activity that may occur in epileptogenic foci adjacent to upcoming ictal events can potentially indicate epileptic conditions that are modulated by inhibitory interneuronal activity. However, how inhibitory neuronal activities are related to blood flow changes in the absence of ongoing seizures, such as during interictal hypoperfusion, is not fully understood yet. Moreover, the relative contribution of excitatory and inhibitory neuron activity to vascular responses between different epileptic states is still unclear.

We propose that a comprehensive examination of excitatory and inhibitory neurons as well as vascular activity is needed to thoroughly elucidate the NVC underlying different epileptic states. We therefore sought to investigate whether vascular responses caused by different epileptic states can be used as biomarkers of pathological states in excitatory and inhibitory neurons in epileptogenic foci. In this study, we conducted real-time *in vivo* measurements of CBF, cortical vessel diameter, and excitatory and inhibitory neuronal activity. We used a 4-aminopyridine (4-AP) seizure model that is known to reliably induce stereotypical focal seizures with sufficient interictal and ictal intervals.<sup>20,21,26,30</sup> Additionally, the 4-AP model allowed us to fully explore the dynamics of neurovascular events in a territorially well-defined seizure focus.<sup>29,42</sup> Local field potential (LFP) recordings were also simultaneously performed to verify seizure events, and to investigate neural correlates that are related to neuronal and vascular dynamics.

## Materials and methods

### Animals

All experimental procedures were approved by the Sungkyunkwan University Institutional Animal Care and Use Committee and were conducted in accordance with the Guide for the Care and Use of Laboratory Animals of the Animal Protection Law & the Laboratory Animal Act set by the Korea Animal and Plant Quarantine Agency and the Korea Ministry of Food and Drug Safety. We used adult male C57BL/6 mice ( $n=20$ ; Orient Bio, South Korea), male Thy1-GCaMP6f mice ( $n=10$ , C57BL/6J-TgGP5.17DKim/J, stock no.025939, Jackson Laboratory, USA) and adult male C57BL/6 mice ( $n=10$ ; Orient Bio) with viral expression of GCaMP6f (AA9-mDlx-GCaMP6f-Fishell-2, plasmid#83899, Addgene, USA). All mice were maintained under a 12-h dark/light cycle, 24–25°C temperature and 50–60% humidity. Experiments were carried out on 10- to 14-week old mice.

### Animal surgery for *in vivo* experiments

Surgical and experimental procedures were performed as shown in Figure 1(a). Mice were initially anesthetized with 2.5% isoflurane in an induction chamber, and anesthesia was maintained with 1.2% isoflurane after each mouse was transferred to a stereotaxic frame (Kopf Instruments, USA). Body temperature was maintained at approximately 37°C using a temperature-controlled heating pad (DC temperature control system, FHC, USA). After an incision was made in the skin over the right hemisphere, a 2-mm-diameter circular craniotomy was carefully performed over the somatosensory cortex (0.5–2.5 mm posterior and 1–3 mm lateral to bregma) using a dental drill (Ram Products, Microtorque II, USA). The dura mater remained intact. The exposed cortex was covered with a glass coverslip (4 × 4 mm, Deckglaser, Germany), but a small space was left on the lateral side to allow for insertion of a microelectrode and a glass pipette (Supplementary Figure 1(a,b)). A metal holding frame was then glued to the skull to (1) minimize head motion during imaging and (2) adjust the tilt of the head so that the brain surface inside the imaging window was perpendicular to the microscope objective axis. For further experiments, anesthesia was then switched to urethane (1.25 g/kg, *i.p.*). Urethane anesthesia has been extensively used for NVC studies.<sup>29,43–46</sup> It is known to preserve excitatory and inhibitory synaptic transmission<sup>47</sup> and autoregulation of CBF.<sup>48</sup> Throughout the experiments, we continuously monitored the physiological parameters of the mice

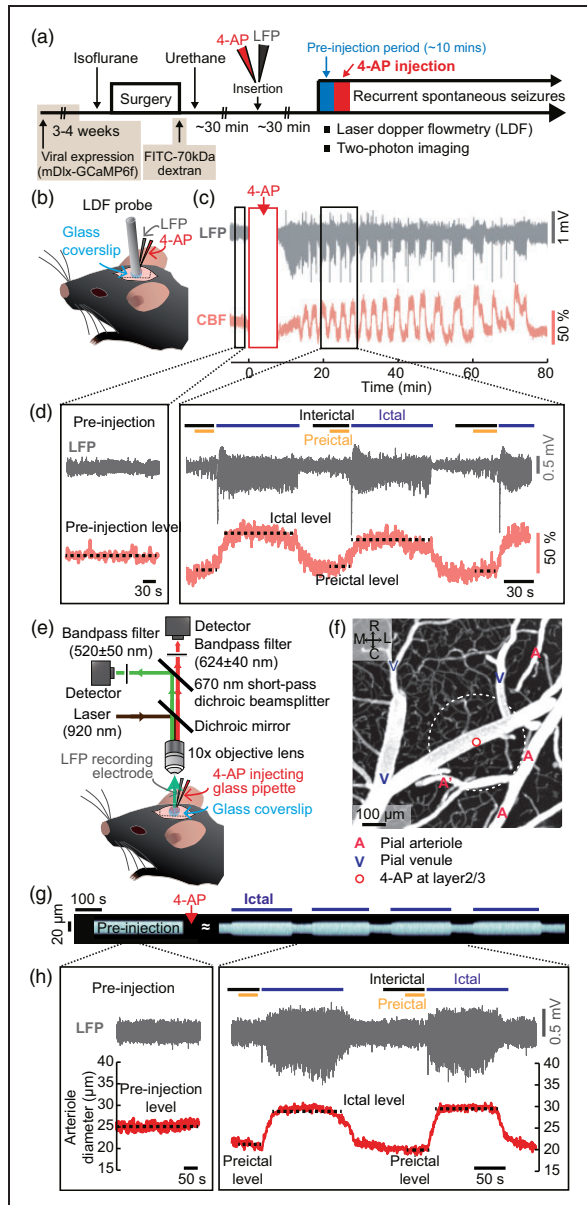


**Figure 1.** Dynamics of CBF and vascular diameter during recurrent spontaneous seizures. (a) Schematic representation of the experimental procedures. Four different sets of experiments were separately conducted in different animal groups: one for LDF recording (wild-type C57BL/6 mice) and the others for two-photon microscopic imaging of cortical pial vessels (wild-type C57BL/6 mice), excitatory (C57BL/6J-Tg-Thy1GCaMP6f.17) and inhibitory calcium activity assessment (wild-type C57BL/6 mice injected with AAV9-mDlx-GCaMP6f virus, 3–4 weeks prior to the experiment). (b) Schematic of the placement of the LDF recording probe with a glass pipette and an LFP recording probe. (c) Examples of LFP and CBF traces over time showing that seizures repeatedly occurred at intervals of several tens of seconds or several minutes for about an hour. (d) Magnified views of LFP and CBF traces during the pre-injection period and during recurrent seizures (square boxes in (c)). (e) Diagram of the two-photon imaging system. (f) Two-photon z-stack projection image up to  $\sim 100\ \mu\text{m}$  from the pial surface. A: arteriole, V: venule. R:

(heart rate: 520–580 bpm,  $\text{SpO}_2$ : 98–99%, respiratory rate: 165–180 r/min) to ensure that stable physiological conditions were maintained under urethane anesthesia.

### Virus injection

For two-photon imaging of GCaMP6f in inhibitory neurons, we intracortically injected AA9-mdlx-GCaMP6f-Fishell-2<sup>49</sup> ( $0.92 \times 10^{13}$  GC/ml) into the somatosensory cortex 3–4 weeks prior to the surgical procedures described above. C57BL/6 mice were also anesthetized via inhalation of 2.5% isoflurane in an induction chamber and were maintained under anesthesia with 1.5% isoflurane during the injection. Two small holes (0.25 mm diameter,  $-1$  to  $-2$  mm posterior and 1 mm lateral to the bregma) were made in the right hemisphere avoiding the large pial vessels. The tip of a beveled ( $40^\circ$  angle) glass micropipette (outer diameter (OD) of 15–20  $\mu\text{m}$ ) was inserted into layer 2/3 of the somatosensory cortex with a micromanipulator (Eppendorf, Germany). The virus solution (1/2 diluted in saline, 800 nl) was injected using a syringe pump (80 nl/min, Harvard Apparatus, USA). The holes were then covered with dental resin (OA2, Dentkist Inc., South Korea) and the skin was sutured.

### Electrophysiological recording and seizure model establishment

A tungsten microelectrode (300–500 k $\Omega$ , FHC, USA) was used for LFP recordings, and a glass micropipette was made for induction of seizure events via intracortical injection of 4-AP (15 mM in sterile saline, Sigma, USA) mixed with Alexa594 (10  $\mu\text{M}$ , Thermo Fisher, USA). A glass pipette with a tip diameter of 20–30  $\mu\text{m}$  was made from a glass capillary tube (OD: 1.0 mm, inner diameter (ID): 0.50 mm, borosilicate glass, Sutter Instrument, USA) using a micropipette puller (P-1000, Sutter Instrument). While viewing the cortex through a microscope objective lens, a microelectrode and a glass micropipette filled with the 4-AP solution were carefully inserted into the cortex ( $25^\circ$  angle) to a depth of  $\sim 350\ \mu\text{m}$  beneath the pial surface. The distance between the microelectrode tip and the glass pipette was up to 500  $\mu\text{m}$  in all

### Figure 1. Continued

rostral, C: caudal, M: medial and L: lateral. The tip of the glass pipette was located  $\sim 350\ \mu\text{m}$  below the pial surface, which is marked with a white dotted line. (g) Stacks of perpendicular lines over time on one branch point of the pial arteriole indicated as A' in (f). (h) Example of LFP signals and pial arteriole diameter changes during the pre-injection period and during recurrent seizures.

experiments. The raw electrophysiological data were amplified and acquired at 40,000 Hz using an Omniplex recording system (Plexon, USA). The LFP signals were then acquired via downsampling to 1,000 Hz and filtering with 0.5-Hz high-pass and 200-Hz low-pass filters. After pre-injection baseline data were acquired for 10 min, the 4-AP solution was slowly injected (80 nl/min) using an infusion pump (Pump 11 Pico Plus Elite, Harvard Apparatus). The mixture of 4-AP with Alexa 594 enabled visualization of the glass pipette during the insertion and of the diffusion area during the infusion (500 nl, 80 nl/min; Supplementary Figure 1(c)). The 4-AP injection reliably induced recurrent spontaneous seizures that repeatedly occurred at intervals of several tens of seconds to several minutes and could be verified by LFP recording (Supplementary Figure 1(d)).

### Laser Doppler flowmetry

CBF changes were measured by using a Laser Doppler flowmetry (LDF) probe (wavelength: 780 nm, probe diameter, 450  $\mu\text{m}$ , Perimed, PeriFlux System 5000, Sweden). The LDF probe was placed on the cortical surface, avoiding the large pial vessels, and separated from the LFP recording microelectrode by  $\sim 200 \mu\text{m}$ . The LDF signals were sampled at 1 kHz and were digitally acquired using a Plexon system that allowed simultaneous measurement of the LDF signals with the LFPs. To assess preictal CBF changes, the measured LDF signals were normalized to the averaged CBF level of the 5- or 10-min period before the 4-AP was injected.

### In vivo two-photon imaging

Two-photon imaging was conducted to measure changes in either cortical vascular diameter or neural activity. For two-photon vessel imaging, fluorescein isothiocyanate (FITC)-labeled dextran (MW = 70 kDa, FD-70S, Sigma) was used to visualize the cortical vasculature (5%, 1.5  $\mu\text{l/g}$ , through the retro-orbital sinus).<sup>50</sup> We chose an area of the somatosensory cortex in which at least two penetrating arterioles and venules were observed. Calcium imaging of neural activity was performed in mice expressing GCaMP6f in excitatory or inhibitory neurons in the somatosensory cortex. Images were obtained using a two-photon laser scanning microscopy system (TCS SP8 MP, Leica, Germany) equipped with a broadly tunable Ti:sapphire laser (680–1080 nm, 80 MHz, 140 fs pulse width, Chameleon Vision II, Coherent, USA). A 10 $\times$  objective lens (Leica, HCX APO L, NA = 0.30) was used with a 920-nm tuned laser to excite the fluorescent signals. Bandpass filters at 520/50 nm and 585/40 nm

were used to collect green (FITC or GCaMP6f) and red (Alexa594 mixed with the 4-AP solution) fluorescence, respectively, at a pixel resolution of 1.73  $\mu\text{m}$ . Focusing at a depth of 250–300  $\mu\text{m}$  (layer 2/3), images were acquired at 2 Hz for surface vascular imaging and at 5 Hz or 10 Hz for calcium imaging. The imaging area included the tip of the 4-AP glass pipette but not the microelectrode tip because direct exposure of metal microelectrodes to focused Ti:sapphire laser light creates photovoltaic artifacts.<sup>38</sup> Thus, the electrode tip was positioned rostrally or caudally near the border of the imaged area to avoid artifacts (Supplementary Figure 1 (b) and (c)).

### Data analysis

All data were analyzed using Fiji (ImageJ, USA), custom-written code in MATLAB (Mathworks, USA) and Chronux (<http://chronux.org/>). To ensure that consecutive ictal events were treated as isolated episodes, seizure events with intervals of less than 40 s were excluded from further analysis.<sup>26,28,34</sup> The neural recordings were 0.5–150-Hz bandpass filtered using a third-order Butterworth filter. Seizure onset was defined as the time point at which LFP amplitudes increased two standard deviation (SD) above the preictal baseline. The offset was defined as the time point at which the signal returned to within 2 SD of the preictal baseline. Seizure onset and offset were then confirmed by visual inspection and adjusted manually. A time course of the power spectral density (PSD) was calculated by applying a multitaper transformation (sliding window: 1 s, bin: 100 ms). The PSDs were summed in five distinct frequency ranges: 1–4 Hz ( $\delta$ -band), 4–7 Hz ( $\theta$ -band), 7–13 Hz ( $\alpha$ -band), 13–30 Hz ( $\beta$ -band), and 30–100 Hz ( $\gamma$ -band).

The detailed methods for postprocessing of the imaging data are described in the Supplementary Material. The preictal CBF and diameter changes (%) measured during the 10 s prior to each seizure onset were normalized by the averaged pre-injection baseline. The ictal CBF and diameter changes (%) were calculated by normalizing the ictal CBF levels and diameters by the average preictal CBF level and diameter. The arteriole or venule changes from different segments in each field of view (FOV) were averaged for each seizure. The GCaMP6f signals over time were calculated as  $\Delta F/F = (F - F_0)/F_0$ , where  $F_0$  and  $F$  represent the baseline fluorescence (the averaged fluorescence of either the 10-min pre-injection or the preictal period) and the fluorescence over time, respectively. To quantify the oscillating activity during the preictal periods, we counted peaks only when they appeared more than 400 ms after the previous one or were more than 0.2-fold higher than the basal preictal level. To analyze

neuronal synchrony, the correlation coefficients of the  $\Delta F/F$  signals were calculated (1 s window with a 1 s step) for all pairs of the neuron regions of interest (neuron ROIs) for each seizure.

### Study design and statistics

The study design and reporting followed the ARRIVE (Animal Research: Reporting In Vivo Experiments) guidelines. The sample sizes were determined to detect over 30% differences between mean values (coefficient of variance = 0.2–0.5, power = 80%,  $\alpha = 0.05$ ). We conducted normality tests with the Shapiro-Wilk test for all data sets (IBM SPSS Statistics 19, USA). Depending on the results of the normality test, we used either an independent *t*-test or the Mann-Whitney *U* test to examine differences between two independent samples. We used either a paired *t*-test or the Wilcoxon signed-rank test when comparing two dependent samples. Likewise, according to the normality test results, we calculated either Pearson's or Spearman's correlation coefficient to examine a linear relationship between two variables, and linear regression models were fitted using the ordinary least squares method. \*\*\*, \*\*, and \* indicate  $p < 0.001$ , 0.01 and 0.05, respectively. The data throughout the paper are displayed as mean  $\pm$  SD or as the median with 25th–75th percentiles. The numbers of trials and animals used for the data analyses are also described in the figure legends.

## Results

### *Ictal increases in CBF and vessel diameter are correlated with its preceding preictal CBF and diameter that are associated with $\gamma$ -band LFP power*

As shown in Figure 1(a), we first investigated real-time CBF and vessel diameter changes by LDF recording (Figure 1(b)) and by two-photon imaging (Figure 1(e)) with concurrent recording of LFP signals. For vessel imaging, FITC-labeled 70-kDa dextran was retro-orbitally injected into wild-type C57BL/6 mice to visualize the cortical vasculature. Prior to 4-AP injection, the basal CBF level and vessel diameter were measured for approximately 10 min. Within several minutes following the 4-AP injections, recurrent spontaneous seizures were generated, and CBF changes were tightly linked to different epileptic states (Figure 1(c)). In accordance with other reports using the 4-AP model, we used the term “ictal” in the context of seizure activity and “interictal” to indicate the periods between two consecutive ictal events.<sup>21,26,28,34</sup> The “preictal” period, as part of the interictal period, was also separately designated as the 30-s time period immediately preceding each seizure onset<sup>21,26</sup>

(Figure 1(d) and Supplementary Figure 1(d)). For further analysis, we focused on two epileptic states, the preictal and ictal states, and examined how the two states are related from the perspective of NVC.

Compared to the CBF levels before injection, the CBF levels during interictal periods, including preictal states, were lower, while those during ictal states were higher (Figure 1(d)). In addition, termination of recurrent seizures that were generally maintained for approximately 60–90 min was associated with a reduction in CBF level (Supplementary Figure 2(a) and (b)), and LFP amplitudes during recurrent seizures were negatively correlated with postictal CBF reductions (Supplementary Figure 2(c)). No epileptiform activity was observed after saline injection alone (sham control), and there were no apparent changes in LFP, CBF or heart rate over time (Supplementary Figure 3(a)). We also confirmed that the anesthesia conditions were stable in sham control and 4-AP injected mice throughout the experiments (Supplementary Figure 3(b)). In line with the CBF changes, the arteriole diameters were lower during interictal and preictal states than before injection and were increased during ictal events (Figure 1(g) and (h)).

To estimate preictal CBF and diameter changes, each CBF and diameter value during the 10 s prior to seizure onset was normalized by its respective 10-min-averaged pre-injection level (Figure 2(a), preictal change (%)). To estimate ictal CBF and diameter changes, the average CBF and diameter during each seizure event were normalized by the respective preceding preictal values (Figure 2(a), ictal change (%)). Overall, the preictal CBF level fell by  $27.98 \pm 16.18\%$ , and the ictal CBF increased by  $69.00 \pm 52.47\%$  (Figure 2(b)). The ictal CBF responses were comparable to those shown in other reports.<sup>28,29</sup> The preictal arteriole diameter decreased by  $22.71 \pm 13.14\%$  and the ictal diameter increased by  $18.47 \pm 11.76\%$  (Figure 2(d)). Venule diameter changes were used as references to confirm that the observed changes in arteriole diameter were not attributable to motion artifacts or focal plane drifts (Supplementary Figure 4(a) and (b)). Interestingly, the preictal CBF level was highly negatively correlated with the subsequent ictal CBF increase (Figure 2(c); Spearman's  $r = -0.644$ ,  $p < 0.001$ ,  $R^2 = 0.572$ ), showing that a larger decrease during the preictal period was associated with a larger increase during the ictal period. Likewise, the preictal arteriole diameter, which was variable over time (Supplementary Figure 4(c)), was negatively correlated with subsequent ictal dilation (Figure 2(e); Spearman's  $r = -0.848$ ,  $p < 0.001$ ,  $R^2 = 0.746$ ). In other words, greater reductions in CBF and arteriole diameter during the preictal state were associated with a higher CBF response and vasodilation during the subsequent ictal state,

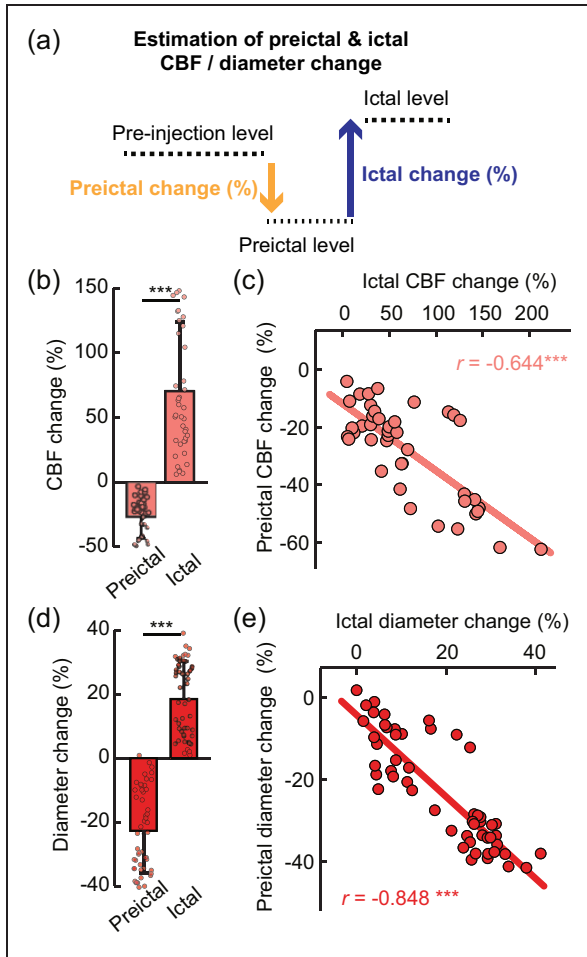


**Figure 2.** Preictal and ictal changes in CBF and arteriole diameter. (a) Schematic of changes in CBF and vessel diameter during the pre-injection, preictal and ictal periods. To estimate preictal changes (%), each preictal level was normalized by the average pre-injection level. To estimate ictal change, the ictal level was averaged during the full ictal period, and this value was then normalized with the preceding preictal level. (b) Preictal ( $-27.98 \pm 16.18\%$ ) and ictal ( $69.00 \pm 52.47\%$ ) CBF changes (total number of seizures = 42,  $n = 5$ , mean  $\pm$  SD,  $^{***}p < 0.001$  by Wilcoxon signed-rank test). (c) Relationship of the preictal CBF change with the ictal CBF change (total number of seizures = 42,  $n = 5$ , Spearman's  $r = -0.644$ ,  $^{***}p < 0.001$ ,  $R^2 = 0.572$ ). (d) Preictal ( $-22.71 \pm 13.01\%$ ) and ictal ( $18.47 \pm 11.65\%$ ) arteriole diameter changes (total number of seizures = 53,  $n = 8$ , mean  $\pm$  SD,  $^{***}p < 0.001$  by Wilcoxon signed-rank test). (e) Relationship of the preictal arteriole change with the ictal arteriole change (total number of seizures  $n = 53$ ,  $n = 8$ , Spearman's  $r = -0.848$ ,  $^{***}p < 0.001$ ,  $R^2 = 0.746$ ).

respectively. To characterize the neural correlates of the preictal vascular changes, we then compared them with concurrently measured LFP signals. The preictal vascular changes were most highly correlated with the power of the  $\gamma$ -band among the different neural bands of preictal LFP signals (Table 1), and a lower  $\gamma$  power was correlated with a larger reduction in the preictal

**Table 1.** Coefficients of correlation (Spearman's  $r$ ) between the preictal LFP power at different neural frequency bands and the preictal arteriole diameter shown in Figure 2(d) and (e).

|           | $\delta$ | $\theta$ | $\alpha$ | $\beta$ | $\gamma$        |
|-----------|----------|----------|----------|---------|-----------------|
| $r$       | 0.165    | 0.459    | 0.298    | 0.365   | 0.529           |
| $p$ Value | 0.238    | 0.01*    | 0.031*   | 0.007** | $6.02e^{-5***}$ |
| $R^2$     | 0.094    | 0.061    | 0.189    | 0.219   | 0.284           |

\* $p < 0.05$ . \*\* $p < 0.01$ . \*\*\* $p < 0.001$ .

vessel diameter. When the seizure strength was estimated by summing the absolute LFP power during each ictal event, a stronger seizure with a higher ictal dilation (Supplementary Figure 5, right; Spearman's  $r = 0.518$ ,  $^{***}p < 0.001$ ,  $R^2 = 0.242$ ) was associated with a larger decrease in arteriole diameter in the preictal period (Supplementary Figure 5, left; Spearman's  $r = -0.377$ ,  $^{**}p = 0.007$ ,  $R^2 = 0.145$ ). Collectively, these data reveal that the potential neural origin of the preictal vascular change is related to the  $\gamma$ -band of LFP signals, and that the preictal level affects the strength of the following seizure.

#### Preictal excitatory and inhibitory neuronal activity during recurrent seizures

We then sought to examine the excitatory and inhibitory neuronal activity levels underlying the preictal vascular changes and LFP  $\gamma$  power by in vivo two-photon calcium imaging. For this, we used transgenic Tg-Thy1-GCaMP6f-GP5.17DKim/J<sup>51</sup> and C57BL/6 mice with viral expression of GCaMP6f under an mdlx promoter (AA9-mDlx-GCaMP6f-Fishell-2).<sup>49</sup> Immunostaining verified GCaMP expression in neurons in the somatosensory cortex (Figure 3(a), (d) and Supplementary Figure 6). In Thy1-GCaMP6f mice, which are known to express GCaMP6f in cortical pyramidal neurons,<sup>51,52</sup> GCaMP6f<sup>+</sup> cells were well overlaid with NeuN<sup>+</sup> signals (Supplementary Figure 6(a)). Under the mDlx promoter, the proportions of PV<sup>+</sup> and SOM<sup>+</sup> neurons in GCaMP6f<sup>+</sup> cells were  $33.57 \pm 9.37\%$  and  $17.09 \pm 3.08\%$  (Supplementary Figure 6(b-d)), respectively, in accordance with previous reports.<sup>49,53</sup> Additionally, GCaMP6f<sup>+</sup> cells were accounted for  $92.48 \pm 9.80\%$  and  $95.01 \pm 4.13\%$  of PV<sup>+</sup> and SOM<sup>+</sup> cells, respectively (Supplementary Figure 6(e)). These results indicate that viral expression under the mDlx promoter is specific to and effective in GABAergic inhibitory neurons. Two-photon GCaMP6f imaging was performed separately in excitatory and inhibitory neurons to avoid overlapping signals between them, especially in neuropils. Spontaneous GCaMP6f signals in excitatory neurons were apparently weaker in both soma and neuropils

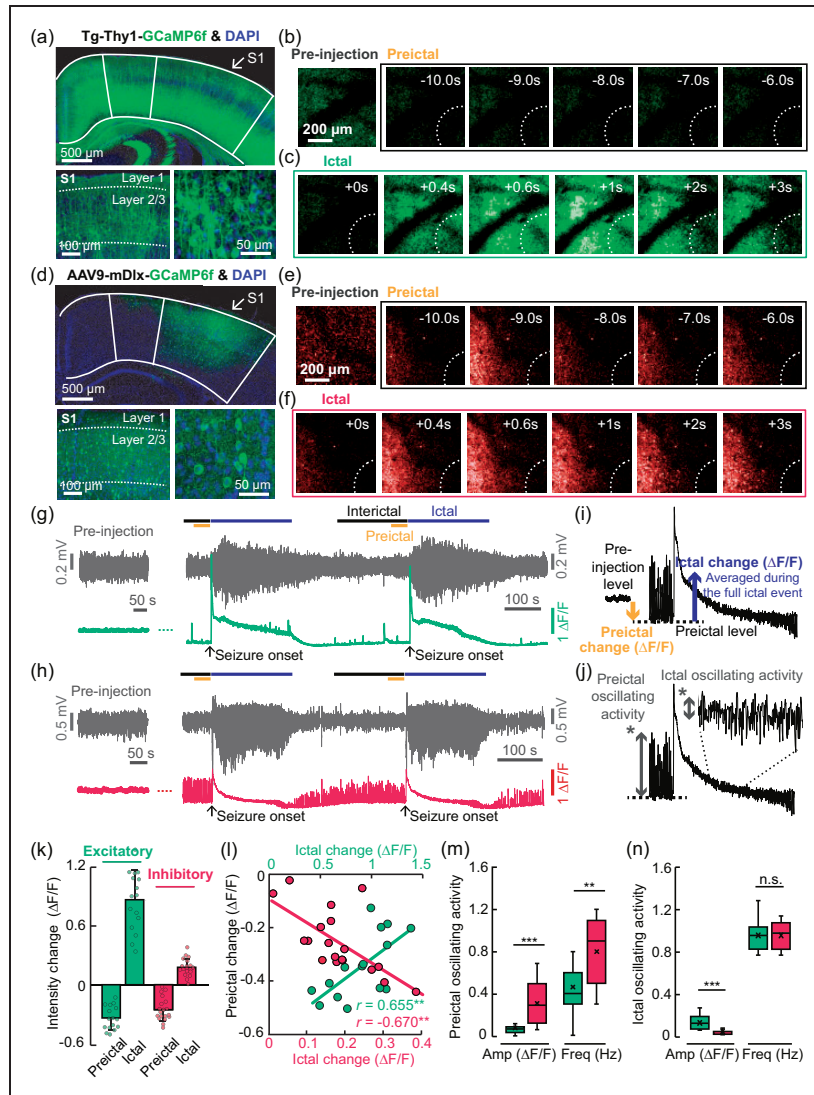


**Figure 3.** In vivo two-photon calcium imaging of excitatory and inhibitory neurons during the pre-injection period and during recurrent spontaneous seizures. (a) Transgenic expression of GCaMP6f under the Thy1 promoter in brain regions including the somatosensory cortex (top) and GCaMP6f expression in layer 2/3 neurons of the somatosensory cortex (bottom, left and right). (b–c) Representative images of spatiotemporal fluorescence changes in excitatory neurons during the pre-injection, preictal and ictal periods. (d) Viral expression of GCaMP6f under the mDlx promoter in the somatosensory cortex (top) and GCaMP6f expression in layer 2/3 neurons of the mouse somatosensory cortex (bottom, left and right). (e–f) Representative images of spatiotemporal fluorescence changes in excitatory and inhibitory neurons during the pre-injection, preictal and ictal periods. (g,h) Examples of LFP signals and GCaMP6f intensity changes (averaged from all the pixels within a range of 200–700  $\mu\text{m}$  from the location of a glass pipette tip) in excitatory (green) and inhibitory (red) neurons. (i,j) Schematic explanation of the calculation of preictal and ictal changes in the GCaMP6f signals. (k) Bar plot of the preictal fluorescence intensity changes in the preictal period (excitatory:  $-0.34 \pm 0.12 \Delta F/F$ , mean  $\pm$  SD; inhibitory:  $-0.25 \pm 0.12 \Delta F/F$ , mean  $\pm$  SD) and ictal period (excitatory:  $0.87 \pm 0.30 \Delta F/F$ , mean  $\pm$  SD; inhibitory:  $0.18 \pm 0.09 \Delta F/F$ , mean  $\pm$  SD). Excitatory: total number of seizures = 16,  $n = 5$ ; inhibitory: total number of seizures = 19,  $n = 4$ . (l) Relationships between preictal basal excitatory and inhibitory activity levels and the following ictal changes (excitatory: Pearson's  $r = 0.655$ ,  $**p = 0.008$ ,  $R^2 = 0.428$ ; inhibitory: Pearson's,  $r = -0.670$ ,  $**p = 0.002$ ,  $R^2 = 0.448$ ). (m,n) Box-whisker diagrams of the amplitudes (Amp) and frequencies (Freq) of the preictal and ictal oscillating activity. Preictal, amplitude,  $***p < 0.01$  by Mann-Whitney U test; preictal, frequency,  $***p < 0.001$  by independent t-test; ictal, amplitude:  $***p < 0.001$  by independent t-test; ictal, frequency: n.s. (no statistical significance) by independent t-test.

during the preictal state than during the pre-injection period (Figure 3(b)) and increased following seizure onset (Figure 3(c)). On the other hand, those in inhibitory neurons showed heterogeneous changes during the preictal period, as indicated by the basal fluorescent levels (Figure 3(e)), and increased following seizure onset (Figure 3(f)). The averaged excitatory signals (fluorescence levels) of 200–700  $\mu\text{m}$  around the injection focus were decreased during interictal and preictal states (Figure 3(g)). Interestingly, the inhibitory signals not only were generally decreased during interictal and preictal states but also had distinct oscillations (Figure 3(h) and Supplementary Movie 1).

In line with the previous methods for quantification of CBF and vessel diameter changes, the preictal signal changes were normalized by the averages during the 10-min pre-injection period, and the ictal changes were normalized by those of the preceding preictal period (Figure 3(i)). The preictal level ( $\Delta F/F$ ) was decreased by  $0.34 \pm 0.12$  and  $0.25 \pm 0.12$  in excitatory and inhibitory neurons, while the ictal change ( $\Delta F/F$ ) was increased by  $0.87 \pm 0.30$  and  $0.18 \pm 0.09$  in excitatory and inhibitory neurons, respectively (Figure 3(k)). Seizure duration and LFP amplitudes in seizure events were similar between the different experiments (Supplementary Figure 7). Lower (i.e. larger reductions in) excitatory neuron preictal activity and inhibitory neuron preictal activity were followed by less and more seizure-evoked activity, respectively (Figure 3(l); excitatory: Pearson's  $r = 0.655$ ,  $**p = 0.008$ ,  $R^2 = 0.428$ ; inhibitory: Pearson's  $r = -0.670$ ,  $**p = 0.002$ ,  $R^2 = 0.448$ ). Moreover, the negative preictal–ictal relationship observed for inhibitory neuronal activity was consistent with the negative preictal–ictal relationship observed for the vascular activity (CBF; Figure 2(c); Spearman's  $r = -0.644$ \*\*\*; arteriole diameter; Figure 2(e); Spearman's  $r = -0.848$ \*\*\*).

When the preictal oscillating activity levels were quantified as shown in Figure 3(j), the amplitudes ( $\Delta F/F$ ) were  $0.09 \pm 0.08$  and  $0.31 \pm 0.18$  in excitatory and inhibitory neurons, respectively, while the frequencies were  $0.46 \pm 0.26$  Hz and  $0.81 \pm 0.30$  Hz (Figure 3(m)), indicating that inhibitory neurons exhibit more apparent oscillating activity than excitatory neurons during the preictal period. From these results, we suppose that excitatory and inhibitory neurons contribute differently to the preictal state, which may affect subsequent seizure events. Additionally, ictal oscillating activity, which was relatively higher in excitatory neurons than in inhibitory neurons (Figure 3(n)), was much lower than preictal inhibitory activity, indicating that oscillating activity is more specific to inhibitory neurons in the preictal state.

### *The level of preictal basal neuronal activity, which is characterized by coherent oscillating inhibitory neuronal activity, is related to the preictal $\gamma$ -band LFP power*

We further explored neuronal activity at the single-soma level. Based on seizure-evoked GCaMP6f intensity changes, a map of cell soma regions (neuron ROIs) was created for each seizure trial as described in Supplementary Figure 8 and in the Supplementary Material. Calcium transients were then extracted from neuron ROIs. To examine whether the oscillating activity resulted from neuronal synchrony, we calculated the correlation coefficients of the calcium transients between all neuronal pairs. During the preictal period, oscillating activity (Figure 4(a) and (b)) and neuronal synchrony (Figure 4(c) and (d)) were apparent in inhibitory soma activity. The averaged correlation values over time (shown as yellow lines) matched well with the oscillating activity of inhibitory neuronal calcium signals (Figure 4(f) and (h)) as opposed to excitatory neuronal calcium signals (Figure 4(e) and (g)).

The preictal inhibitory soma activity exhibited higher neuronal synchrony than excitatory activity (Figure 5(a), preictal), and the oscillation of this activity was also significantly higher and more frequent than that of excitatory activity (Figure 5(b)), suggesting that inhibitory neurons may play more active roles than excitatory neurons in shaping the preictal neural state. During the preictal period, the synchronized activity had a strong positive correlation with oscillating activity (Figure 5(d); excitatory: Spearman's  $r = 0.785$ ,  $***p < 0.001$ ,  $R^2 = 0.915$ ; inhibitory: Spearman's  $r = 0.828$ ,  $***p < 0.001$ ,  $R^2 = 0.603$ ). On the other hand, the correlation of excitatory neuronal activity became stronger than that of inhibitory activity during the ictal periods (Figure 5(a), ictal). Ictal oscillating activity, which was relatively weak (Figure 5(c)), was more highly correlated with the correlation of excitatory neuronal activity than that of inhibitory neuronal activity (Figure 5(e); excitatory: Spearman's  $r = 0.776$ ,  $**p = 0.001$ ,  $R^2 = 0.626$ ; inhibitory: Pearson's  $r = 0.558$ ,  $*p = 0.013$ ,  $R^2 = 0.311$ ). Overall, these findings indicate that oscillating activity is mostly apparent in inhibitory neurons in the preictal state and that oscillating activity is related to neuronal synchrony that is contrasting between excitatory and inhibitory activity in two different epileptic states.

During the preictal state, the power of the oscillating inhibitory activity exhibited a positive linear relationship with the basal inhibitory activity level (Figure 5(f); excitatory: Pearson's  $r = -0.068$ , n.s.,  $R^2 = 0.005$ ; inhibitory: Pearson's  $r = 0.507$ ,  $*p = 0.027$ ,  $R^2 = 0.258$ ) that was previously shown to correlate with the magnitude



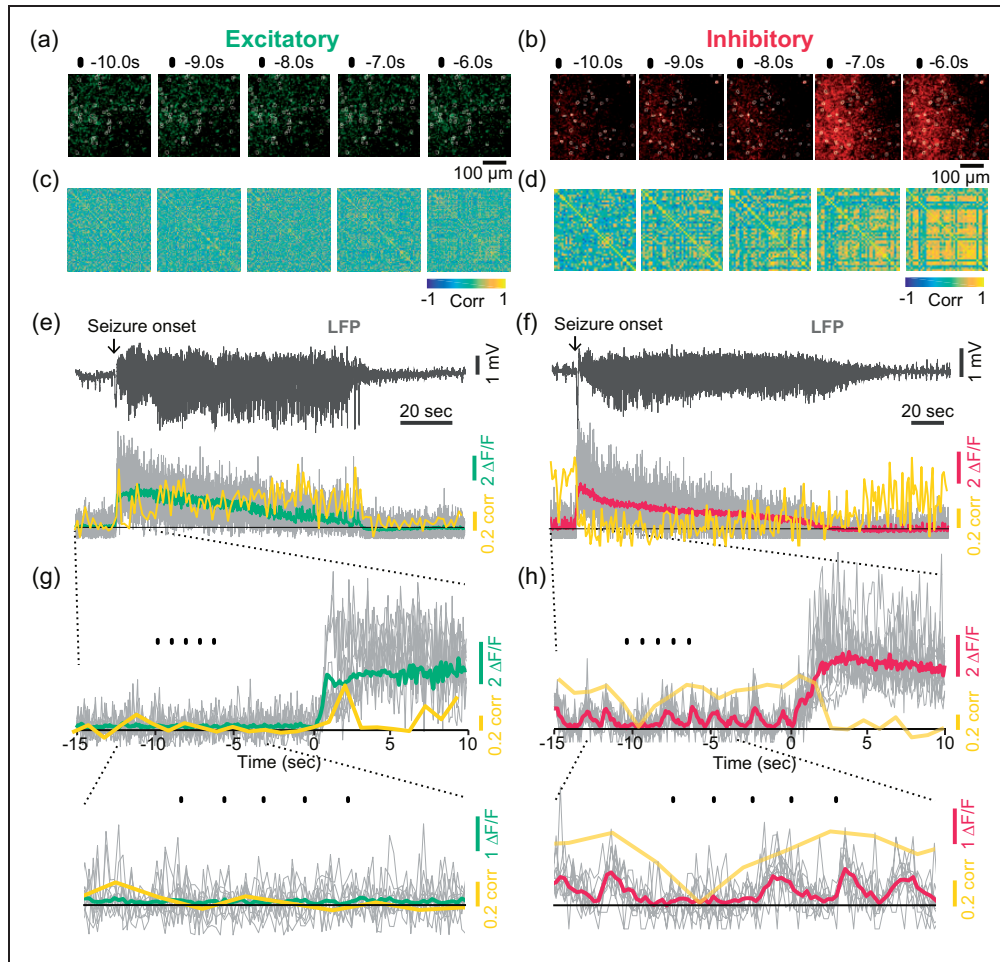


**Figure 4.** Neuronal synchrony of excitatory and inhibitory activity. (a, b) Examples of magnified images showing spatiotemporal activity of excitatory and inhibitory neurons overlaid with the registered neuron ROIs (white contours) for 10.0–6.0 s prior to the seizure onset shown in (e–f). (c, d) Example correlation matrices showing the Pearson's correlation coefficients of all registered neuron ROIs (excitatory: 118 cells, inhibitory: 52 cells) in the same seizure trial shown in (a) and (b). The scale bar indicates the coefficient value between  $-1$  and  $1$ . (e–f) Examples of LFPs and the associated excitatory/inhibitory activity (green or red) overlaid with the correlation coefficients over time (yellow). The correlation values were calculated by averaging the values from all individual pairs of neuron ROIs (cell soma within the range of 200–700  $\mu\text{m}$  range), over time (window: 1 s, step: 1 s). The gray lines indicate individual traces of 10 neuron ROIs that were randomly chosen within the range. (g–h) Magnified traces. The yellow line shows the correlation coefficient values calculated in every 1 s window. The black dots above the traces indicate the same time points shown in (a, c) and (b, d).

of the subsequent ictal response (Figure 3(k)). In other words, more synchronized and oscillating inhibitory activity was linked to a smaller reduction in the basal inhibitory activity level. However, this relationship was not observed for excitatory activity during preictal states. Furthermore, preictal basal excitatory and inhibitory activity levels were also correlated with concurrently measured  $\gamma$ -band LFP power (Figure 5(g); excitatory: Pearson's  $r = -0.611$ ,  $*p = 0.01$ ,  $R^2 = 0.374$ ; inhibitory: Pearson's  $r = 0.495$ ,  $*p = 0.03$ ,  $R^2 = 0.245$ ; the correlation coefficients for other neural bands are shown in Supplementary Tables 1 and 2). Higher  $\gamma$  power was correlated with a greater reduction in the preictal excitatory activity level but a smaller reduction

in the inhibitory activity level. The relationship observed for the inhibitory activity level was consistent with the preictal vascular activity since a higher  $\gamma$  power was associated with a smaller reduction in the preictal arteriole diameter (Table 1).

Overall, we suppose that the preictal vascular activity alongside with the LFP signal  $\gamma$ -band may reflect the relative levels of excitatory and inhibitory neuronal activity during the preictal period, which may imply the magnitude of the following ictal response. In particular, inhibitory neurons may play a major role in shaping the preictal neural state, which is characterized by coherent oscillating inhibitory neuronal activity, regarding the extent of the preictal inhibitory activity

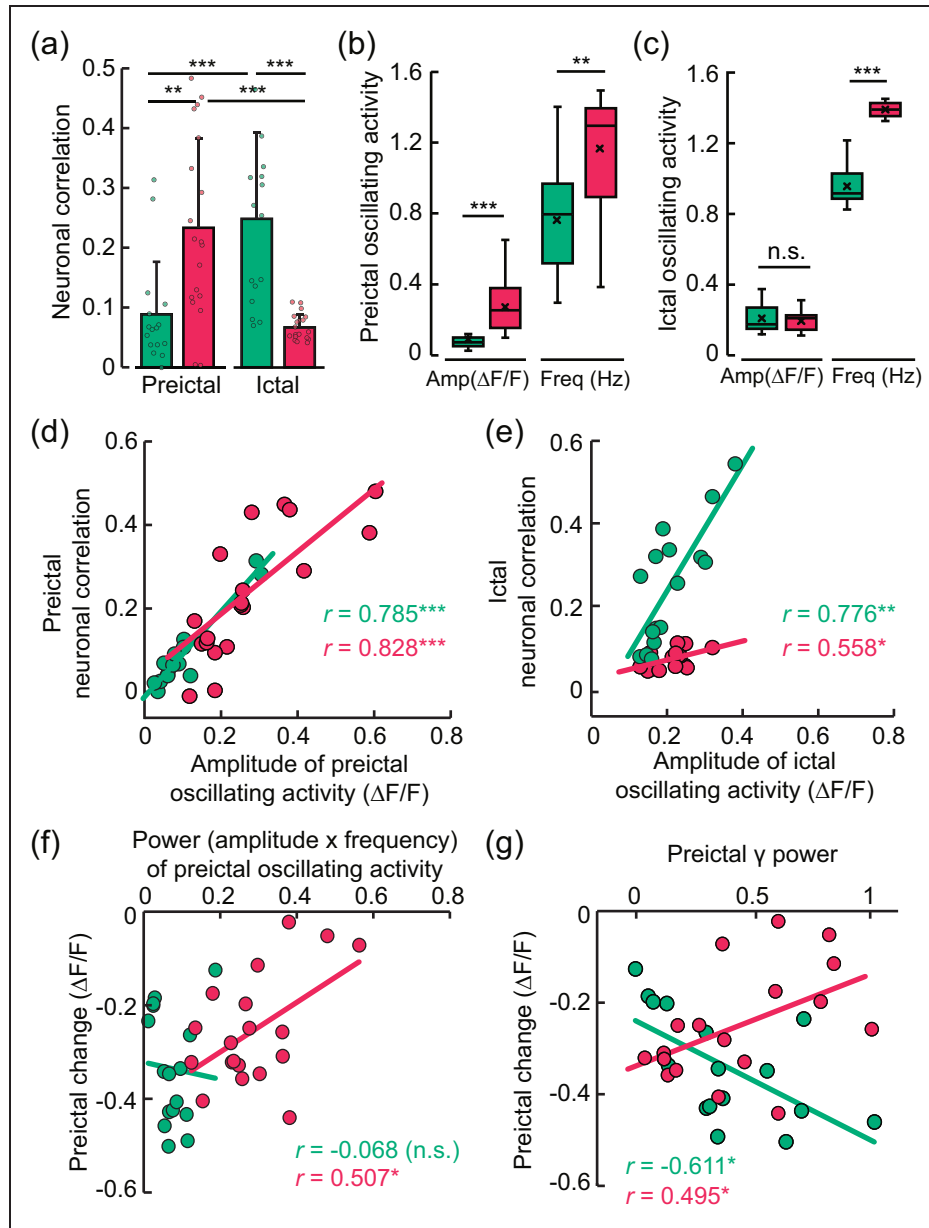


**Figure 5.** Preictal and ictal neuronal synchrony and their relationships with oscillating activity. (a) Correlation coefficients between all pairs of registered neuron ROIs (cell soma within the range of 200–700  $\mu\text{m}$ ) during the preictal and ictal periods. Preictal, excitatory:  $0.09 \pm 0.09$ ; preictal, inhibitory:  $0.23 \pm 0.15$ ; ictal, excitatory:  $0.25 \pm 0.14$ ; ictal, inhibitory:  $0.07 \pm 0.02$  (mean  $\pm$  SD; preictal excitatory & inhibitory,  $**p = 0.001$  by Mann-Whitney U test; ictal excitatory & inhibitory,  $***p < 0.001$  by independent t-test; excitatory preictal & ictal,  $***p < 0.001$  by Wilcoxon signed-rank test; inhibitory preictal & ictal,  $***p < 0.001$  by paired t-test). Excitatory: total number of seizures = 16,  $n = 5$ , total number of cells = 2345, average number of cells in each seizure trial =  $146.56 \pm 23.75$ . Inhibitory: total number of seizures = 19,  $n = 4$ , total number of cells = 1070, average number of cells in each seizure trial =  $48.64 \pm 18.94$ . (b, c) Box-whisker diagrams of the amplitudes ( $\Delta F/F$ ) and frequencies (Hz) of preictal and ictal oscillating activity in excitatory and inhibitory neurons. The boxes represent the 25th–75th percentiles, and the horizontal lines inside the boxes display the median amplitudes (assessed by Mann-Whitney U test) and frequencies ( $**p < 0.001$ ,  $***p < 0.001$ , by Mann-Whitney U test; n.s. indicates no statistical significance). (d, e) Relationships between the correlation coefficients (neuronal correlation) and the amplitudes of the oscillating activity during the preictal (excitatory: Spearman's  $r = 0.785$ ,  $***p < 0.001$ ,  $R^2 = 0.915$ ; inhibitory: Spearman's  $r = 0.828$ ,  $***p < 0.001$ ,  $R^2 = 0.603$ ) and ictal (excitatory: Spearman's  $r = 0.776$ ,  $**p = 0.001$ ,  $R^2 = 0.626$ ; inhibitory: Pearson's  $r = 0.558$ ,  $*p = 0.013$ ,  $R^2 = 0.311$ ) states. (f) Relationship of the preictal basal level (shown in Figure 3(k) and (l)) with the power (amplitude x frequency) of the preictal oscillating activity (excitatory: Pearson's  $r = -0.068$ , n.s.,  $R^2 = 0.005$ ; inhibitory: Pearson's  $r = 0.507$ ,  $*p = 0.027$ ,  $R^2 = 0.258$ ). (g) Relationship between the preictal basal level and the normalized preictal LFP  $\gamma$  power, in excitatory (Pearson's  $r = -0.611$ ,  $*p = 0.01$ ,  $R^2 = 0.374$ ) and inhibitory neurons (Pearson's  $r = 0.495$ ,  $*p = 0.03$ ,  $R^2 = 0.245$ ).

level. On the other hand, excitatory activity shows higher neuronal synchrony than inhibitory activity during the ictal state. Given these results, we suggest that excitatory and inhibitory neurons may contribute differently to shaping two different epileptic neural states, i.e. the preictal and ictal states, and may also affect vascular signals.

## Discussion

In this study, we undertook a detailed investigation of neuronal and vascular activity during recurrent seizures. The main findings of this study were the characterization of vascular, excitatory, and inhibitory activity in two different epileptic states and elucidation of the relationships among these types of activity, as summarized in Figure 6. Moreover, our results suggest that the preictal levels of vascular and neuronal activity may represent the severity of the upcoming ictal event. We believe that this work not only improves understanding of epileptogenesis but also presents a new strategy for prediction of the pathological severity of epilepsy from the perspective of NVC. Altogether, our findings may provide insight into the neuronal basis of the perfusion signals that are often utilized in diagnosing and treating epilepsy patients.

### *Preictal neuronal activity in terms of excitation-inhibition (E/I) balance*

Our data revealed that the basal levels of excitatory and inhibitory activity in preictal states were lower than those in pre-injection periods. Since a balance between excitatory and inhibitory synaptic transmission is important for the maintenance of E/I balance,<sup>54–58</sup> altered preictal neuronal activity may indicate altered synaptic function and E/I imbalance. In the current study, higher ictal activity occurred when the preictal reduction was smaller in excitatory neurons and larger in inhibitory neurons. This preictal condition may indicate greater E/I imbalance, considering that an E/I-imbalanced state is often assumed to generate seizures.<sup>56,59,60</sup> In other words, the differential activity between excitatory and inhibitory neurons may reflect the degree of E/I imbalance. Moreover, E/I balance is precisely modulated by inhibitory neural circuits<sup>53</sup> and is closely related to gamma oscillations.<sup>61–63</sup> Previous reports have also revealed that GABAergic inhibitory interneurons play a key role in the generation of gamma oscillations.<sup>64–67</sup> Similarly, our results showed that weaker  $\gamma$ -band LFP power was correlated with a greater reduction in the basal inhibitory activity level, while the opposite trend was observed for the excitatory activity level. Importantly, only inhibitory neurons exhibited oscillating and synchronized activity during

this period. The degree of oscillating inhibitory activity was correlated with the basal inhibitory activity level. Overall, we suggest that inhibitory neuronal activity plays an important role in shaping preictal neuronal states which may affect the degree of E/I imbalance, and that gamma oscillation strength can imply the degree of neuronal alteration.

### *NVC in different epileptic states*

Our results also showed that CBF and arteriole diameters were generally reduced during preictal states. Such reductions may result from decreased basal activity in both excitatory and inhibitory neurons.<sup>68</sup> However, the degrees of the reductions were variable and were correlated with  $\gamma$ -band LFP power in our study, consistent with other reports showing that gamma oscillations are highly related to resting blood flow changes.<sup>69–71</sup> Greater reductions in vascular activity were associated with lower  $\gamma$  power, which could have been linked to smaller decreases in excitatory activity and larger decreases in inhibitory activity along with less-synchronized activity in inhibitory neurons. Considering that this neuronal condition may result in a greater E/I imbalance, we suppose that the E/I imbalance can be linked to reduced vascular activity during preictal states. Other studies have also revealed that E/I balance is highly related to hemodynamic signals<sup>68</sup> and that E/I imbalance induced by impairment of GABAergic interneuronal activity is accompanied by reduced gamma oscillations and vascular responses.<sup>46</sup> Moreover, GABAergic inhibitory neurons themselves are known to play crucial roles in the regulation of cortical vessel tone and blood flow.<sup>36,38,39,41,72,73</sup> Collectively, these findings suggest that GABAergic interneuronal activity may account for the relationship between the degree of E/I imbalance and vascular responses during preictal states. In addition, gamma oscillation strength may reflect this relationship.

On the other hand, during ictal states, neuronal excitation and synchrony in excitatory neurons were much higher than those in inhibitory neurons in the current study. This may indicate that mainly excitatory neurons contribute to E/I imbalance during ictal states, resulting in neuronal network hyperexcitability.<sup>60,74</sup> Stronger seizures were accompanied by greater vascular responses, consistent with the findings in other reports.<sup>28,29</sup> Increased excitation, which can cause E/I imbalance, may mainly drive vascular responses during ictal states, since activation of NMDA receptors in cortical excitatory neurons releases COX-2 products, resulting in increased blood flow.<sup>75,76</sup>

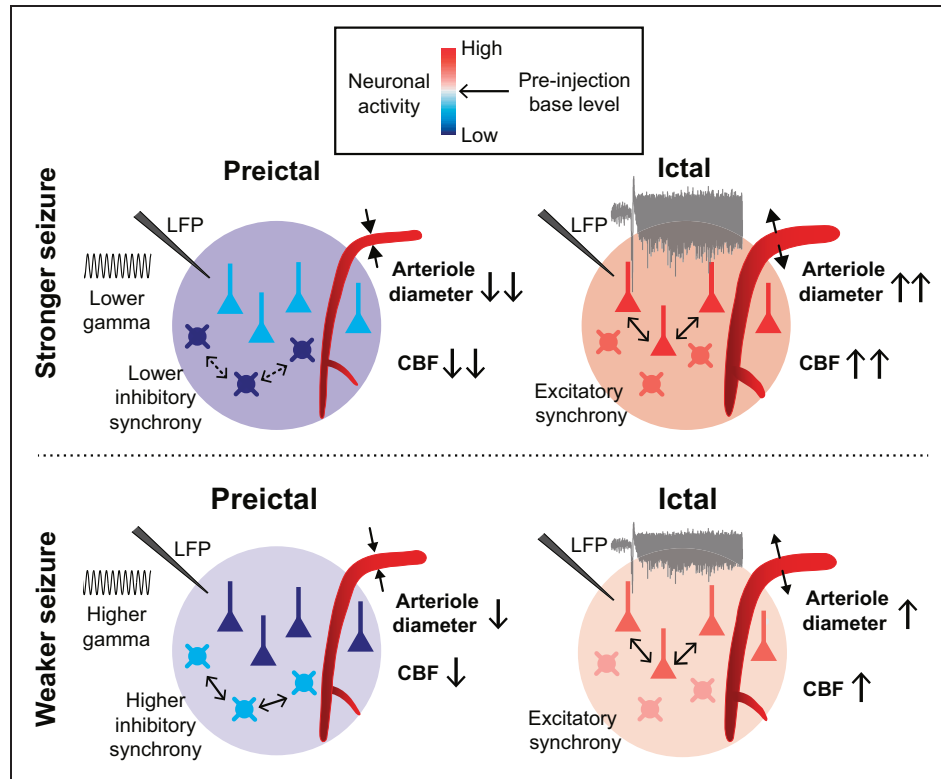


**Figure 6.** Schematic summary showing the relationships between neuronal activity and vascular activity, within and between the preictal and ictal states. Basal CBF, arteriole diameter, and excitatory and inhibitory neuronal activity are altered during the preictal state and are differently correlated with LFP  $\gamma$ -band activity. A lower  $\gamma$ -band during the preictal state is associated with greater reductions in the basal arteriole diameter and the basal inhibitory activity, which are related to lower oscillating and synchronized inhibitory activity. On the other hand, during the preictal state, excitatory oscillating activity is not apparent, and the basal excitatory activity is less reduced. In these cases, the following ictal magnitude is greater, and the ictal state is characterized by higher synchronized activity of excitatory neurons.

Importantly, a recent study has demonstrated that reduced GABA-mediated inhibition can cause ictal propagation via excitatory synaptic pathways<sup>34</sup> and that inhibitory barrages received by pyramidal neurons before they are recruited to ictal events are crucial for opposition of ictal activity.<sup>35,77,78</sup> These findings may explain why the neuronal activity in preictal states, presumed to be driven by GABAergic interneuronal activity, was correlated with that in ictal states, during which neuronal synchrony was higher in excitatory neurons than in inhibitory neurons. Further studies should modulate excitatory and inhibitory neurons in different epileptic states and confirm their roles in the regulation of blood flow in terms of E/I imbalance by precisely measuring their synaptic activity.

#### *Specific subtype of GABAergic inhibitory interneurons as a potential candidate that may account for preictal changes*

Among different subtypes of GABAergic interneurons, PV-expressing interneurons are known as

important regulators of cortical network excitability.<sup>53,79,80</sup> PV neurons can modulate epileptiform activities both *in vitro*<sup>81</sup> and *in vivo*,<sup>21,22,34,82,83</sup> and the recruitment of PV interneurons that precedes the transition to seizure onset has been suggested to play a crucial role in local seizure restraint.<sup>21,23,24,33</sup> In addition, PV interneuronal activity is known to be essential for the generation of gamma oscillations.<sup>63–65</sup> Seizure severity is reduced in mouse epilepsy models when antiepileptic drugs augment interictal  $\gamma$  power in relation to PV interneuronal activity.<sup>84</sup> Consistent with these findings, our data showed that a weaker ictal response was preceded by higher oscillating inhibitory activity, basal inhibitory activity and  $\gamma$  power during the preictal period. Therefore, we suggest that PV interneurons may largely contribute to the preictal neuronal alterations related to gamma oscillations. Moreover, PV interneuronal activity is crucial to the maintenance of E/I balance.<sup>85,86</sup> However, it is unclear how PV interneuronal activity can directly affect preictal vascular activity since its exact role in the modulation of hemodynamics is

controversial.<sup>37,40,87</sup> Considering the abundance of PV interneurons and their connections to other cells in cortical microcircuits,<sup>53,80</sup> these neurons may indirectly affect vascular activity by inhibiting or disinhibiting other neurons that have vasoactive properties.<sup>37,41</sup> Consequently, the roles of different subtypes of inhibitory interneurons in shaping neural and vascular changes during preictal states, as well as their subsequent effects on the following ictal events, should be further investigated.

### **Clinical relevance**

Epilepsy patients frequently show declines in basal perfusion levels despite the absence of ongoing seizures.<sup>6,10,12–14,88,89</sup> Recent studies using animal epilepsy models have described alterations or dysfunction in vascular activity<sup>27,90–92</sup> that may account for the abnormal perfusion signals. Our results suggest that the blood flow changes may also be attributable to alterations in excitatory and inhibitory neuronal activity. Furthermore, since preictal neuronal and vascular activity levels were found to be correlated with the following ictal magnitudes in seizure foci in this study, our observations may provide useful insights for estimation of the pathological severity of epilepsy from the perspective of NVC. Additionally, since the experiments in this study were conducted within a precisely defined seizure focus, our findings may help better localize epileptogenic foci in clinical data acquired during interictal periods, which constitute most of the lives of epilepsy patients.<sup>93</sup>

### **Limitations**

The current study had several limitations that should be addressed in future research. First, the acute pharmacologic seizures that we induced do not perfectly reproduce the chronic focal seizures of human epilepsy. Although 4-AP-induced seizures in anesthetized mice are known to mimic many of the characteristics of spontaneous ictal activity in human focal epilepsy,<sup>21,34,94</sup> our findings may be specific to the 4-AP model used. It is also likely that a direct pharmaceutical effect of 4-AP contributes in part to basal vascular activity, since 4-AP can block voltage-gated potassium channels expressed on vascular smooth muscle cells. However, if the preictal vascular changes we observed were merely due to a vasoconstricting effect of 4-AP, greater reductions would have been followed by smaller vascular changes induced by the following ictal event. Given that we observed the opposite effect, we believe that pharmaceutical-induced vasoconstriction did not confound our observations regarding the preictal-to-ictal neurovascular relationship. Further study is

required to confirm our findings in other epilepsy models, including chronic epilepsy. Additionally, only male mice were used in this study. Sex-dependent effects on excitatory and inhibitory neuronal activity could be an interesting topic for investigation since sex hormones and neurosteroids can affect neuronal excitability and GABA-mediated inhibition, thus causing differences in seizure susceptibility.<sup>95–100</sup> Another interesting point for further investigation is the use of anesthetics. We carried out experiments under anesthesia to avoid the stress of a series of prolonged tonic-clonic seizures in awake mice and because the fundamental characteristics of the general neural activity patterns of cortical seizures are consistent across anesthesia and wakefulness.<sup>20</sup> Urethane anesthesia used in this study is known to preserve excitatory and inhibitory synaptic transmission<sup>47</sup> and to provide a stable state of anesthesia for assessment of NVC.<sup>29,43,44</sup> However, our findings could differ from the situation in the awake state due to different neurovascular properties between anesthesia and wakefulness as suggested by other reports.<sup>101,102</sup> Thus, neuronal and vascular dynamics should be further investigated in awake mice.

### **Conclusion**

To our knowledge, this is the first comprehensive characterization of neuronal and vascular activity, including CBF, vascular diameter, and excitatory and inhibitory neuronal activity, in seizure foci. Based on our results, we suggest that excitatory and inhibitory neurons play different roles in shaping different epileptic states and the associated hemodynamic changes. Our findings provide useful information regarding perfusion changes that are associated with pathological brain states induced by focal epilepsy. Furthermore, they may be applicable to pathological states in other brain diseases because epileptic seizures are phenomena shared by many neurological disorders.

### **Funding**

The author(s) disclosed receipt of the following financial support for the research, authorship, and/or publication of this article: This work was supported by the Institute for Basic Science (IBS-R015-D1), the National Research Foundation of Korea (NRF) funded by the Korean government (MSIT) (No. 2014H1A2A1020612, 2020R1A2C1012017), Basic Science Research Program through the NRF funded by the Ministry of Education (No. 2017R1A6A1A03015642), and the Industrial Strategic Technology Development Program funded by the Ministry of Trade, Industry & Energy (No. 10076675).

## Acknowledgement

We thank Hyesook Lee for her help with immunostaining and Kayoung Han and Jiwoong Min for their helpful discussions and comments on the manuscript.

## Declaration of conflicting interests

The author(s) declare no potential conflicts of interest with respect to the research, authorship, and/or publication of this article.


## Data availability

Requests for further information, resources and reagents should be directed to and will be fulfilled by the corresponding author, Dr. Minah Suh. All relevant data are available from the corresponding author upon reasonable request. The custom-written MATLAB codes used for the analysis are also available from the corresponding author upon reasonable request for the purposes of academic research.

## Authors' contributions

H-KL and MS designed the research; H-KL, NY, and SB performed the experiments; H-KL, NY, and B-MK analyzed the data; H-KL and MS wrote the manuscript; Y-MS and S-GK participated in discussions and provided expertise.

## ORCID iD

Hyun-Kyoung Lim  <https://orcid.org/0000-0003-1818-420X>

## Supplemental material

Supplemental material for this article is available at the journal website: <http://journals.sagepub.com/home/jcb>.

## References

1. Yoo RE, Yun TJ, Yoon BW, et al. Identification of cerebral perfusion using arterial spin labeling in patients with seizures in acute settings. *PLoS One* 2017; 12: e0173538.
2. Oishi M, Ishida G, Morii K, et al. Ictal focal hyperperfusion demonstrated by arterial spin-labeling perfusion MRI in partial epilepsy status. *Neuroradiology* 2012; 54: 653–656.
3. Toledo M, Munuera J, Salas-Puig X, et al. Localisation value of ictal arterial spin-labelled sequences in partial seizures. *Epileptic Disord* 2011; 13: 336–339.
4. Kim S and Mountz JM. SPECT imaging of epilepsy: an overview and comparison with F-18 FDG PET. *Int J Mol Imag* 2011; 2011: 813028.
5. Pizzini F, Farace P, Zanoni T, et al. Pulsed-arterial-spin-labeling perfusion 3T MRI following single seizure: a first case report study. *Epilepsy Res* 2008; 81: 225–227.
6. Calcagni ML, Giordano A, Bruno I, et al. Ictal brain SPET during seizures pharmacologically provoked with pentylentetrazol: a new diagnostic procedure in drug-resistant epileptic patients. *Eur J Nucl Med Mol Imaging* 2002; 29: 1298–1306.
7. Weil S, Noachtar S, Arnold S, et al. Ictal ECD-SPECT differentiates between temporal and extratemporal epilepsy: confirmation by excellent postoperative seizure control. *Nucl Med Commun* 2001; 22: 233–237.
8. Kaiboriboon K, Bertrand ME, Osman MM, et al. Quantitative analysis of cerebral blood flow patterns in mesial temporal lobe epilepsy using composite SISCOM. *J Nucl Med* 2005; 46: 38–43. 2005/01/06.
9. Guo X, Xu S, Wang G, et al. Asymmetry of cerebral blood flow measured with three-dimensional pseudo-continuous arterial spin-labeling mr imaging in temporal lobe epilepsy with and without mesial temporal sclerosis. *J Magn Reson Imaging* 2015; 42: 1386–1397.
10. Boscolo Galazzo I, Storti SF, Del Felice A, et al. Patient-specific detection of cerebral blood flow alterations as assessed by arterial spin labeling in drug-resistant epileptic patients. *PLoS One* 2015; 10: e0123975.
11. Misko J, Jurkiewicz E, Bekiesinska-Figatowska M, et al. Usefulness of coregistration and post-processing of MR and interictal SPECT images for localization of epileptogenic focus in children - preliminary report. *Pol J Radiol* 2011; 76: 7-14. 2012/07/18.
12. Pendse N, Wissmeyer M, Altrichter S, et al. Interictal arterial spin-labeling MRI perfusion in intractable epilepsy. *J Neuroradiol* 2010; 37: 60–63.
13. Lim YM, Cho YW, Shamim S, et al. Usefulness of pulsed arterial spin labeling MR imaging in mesial temporal lobe epilepsy. *Epilepsy Res* 2008; 82: 183–189.
14. Wolf RL, Alsop DC, Levy-Reis I, et al. Detection of mesial temporal lobe hypoperfusion in patients with temporal lobe epilepsy by use of arterial spin labeled perfusion MR imaging. *AJNR Am J Neuroradiol* 2001; 22: 1334–1341.
15. Tamber MS and Mountz JM. Advances in the diagnosis and treatment of epilepsy. *Semin Nucl Med* 2012; 42: 371–386.
16. Kumar A and Chugani HT. The role of radionuclide imaging in epilepsy. Part 1: Sporadic temporal and extratemporal lobe epilepsy. *J Nucl Med* 2013; 54: 1775–1781.
17. Theodore WH. Presurgical Focus Localization in Epilepsy: PET and SPECT. *Semin Nucl Med* 2017; 47: 44–53.
18. Elkins KC, Moncayo VM, Kim H, et al. Utility of gray-matter segmentation of ictal-Interictal perfusion SPECT and interictal (18)F-FDG-PET in medically refractory epilepsy. *Epilepsy Res* 2017; 130: 93–100.
19. Berdyeva TK, Frady EP, Nassi JJ, et al. Direct imaging of hippocampal epileptiform calcium motifs following kainic acid administration in freely behaving mice. *Front Neurosci* 2016; 10: 53.
20. Wenzel M, Hamm JP, Peterka DS, et al. Reliable and elastic propagation of cortical seizures in vivo. *Cell Rep* 2017; 19: 2681–2693.
21. Wenzel M, Hamm JP, Peterka DS, et al. Acute focal seizures start as local synchronizations of neuronal ensembles. *J Neurosci* 2019; 39: 8562–8575.

22. Khoshkhoo S, Vogt D and Sohal VS. Dynamic, cell-type-specific roles for GABAergic interneurons in a mouse model of optogenetically inducible seizures. *Neuron* 2017; 93: 291–298.
23. Schevon CA, Weiss SA, McKhann G Jr., et al. Evidence of an inhibitory restraint of seizure activity in humans. *Nat Commun* 2012; 3: 1060.
24. Cammarota M, Losi G, Chiavegato A, et al. Fast spiking interneuron control of seizure propagation in a cortical slice model of focal epilepsy. *J Physiol* 2013; 591: 807–822.
25. Zhang C, Tabatabaei M, Belanger S, et al. Astrocytic endfoot Ca(2+) correlates with parenchymal vessel responses during 4-AP induced epilepsy: an in vivo two-photon lifetime microscopy study. *J Cereb Blood Flow Metab* 2017; 39: 260–271.
26. Zhao M, Nguyen J, Ma H, et al. Preictal and ictal neurovascular and metabolic coupling surrounding a seizure focus. *J Neurosci* 2011; 31: 13292–13300.
27. Prager O, Kamintsky L, Hasam-Henderson LA, et al. Seizure-induced microvascular injury is associated with impaired neurovascular coupling and blood-brain barrier dysfunction. *Epilepsia* 2019; 60: 322–336.
28. Zhao M, Ma H, Suh M, et al. Spatiotemporal dynamics of perfusion and oximetry during ictal discharges in the rat neocortex. *J Neurosci* 2009; 29: 2814–2823.
29. Harris SS, Boorman LW, Kennerley AJ, et al. Seizure epicenter depth and translaminar field potential synchrony underlie complex variations in tissue oxygenation during ictal initiation. *Neuroimage* 2018; 171: 165–175.
30. Ma H, Zhao M and Schwartz TH. Dynamic neurovascular coupling and uncoupling during ictal onset, propagation, and termination revealed by simultaneous in vivo optical imaging of neural activity and local blood volume. *Cereb Cortex* 2013; 23: 885–899.
31. Miri ML, Vinck M, Pant R, et al. Altered hippocampal interneuron activity precedes ictal onset. *Elife* 2018; 7: e40750.
32. Muldoon SF, Villette V, Tressard T, et al. GABAergic inhibition shapes interictal dynamics in awake epileptic mice. *Brain* 2015; 138: 2875–2890.
33. Parrish RR, Codadu NK, Mackenzie-Gray Scott C, et al. Feedforward inhibition ahead of ictal wavefronts is provided by both parvalbumin- and somatostatin-expressing interneurons. *J Physiol* 2019; 597: 2297–2314.
34. Liou JY, Ma H, Wenzel M, et al. Role of inhibitory control in modulating focal seizure spread. *Brain* 2018; 141: 2083–2097.
35. Trevelyan AJ, Sussillo D, Watson BO, et al. Modular propagation of epileptiform activity: evidence for an inhibitory veto in neocortex. *J Neurosci* 2006; 26: 12447–12455.
36. Cauli B, Tong XK, Rancillac A, et al. Cortical GABA interneurons in neurovascular coupling: relays for subcortical vasoactive pathways. *J Neurosci* 2004; 24: 8940–8949.
37. Krawchuk MB, Ruff CF, Yang X, et al. Optogenetic assessment of VIP, PV, SOM and NOS inhibitory neuron activity and cerebral blood flow regulation in mouse somato-sensory cortex. *J Cereb Blood Flow Metab* 2019; 40: 1427–1440.
38. Uhlirva H, Kilic K, Tian P, et al. Cell type specificity of neurovascular coupling in cerebral cortex. *Elife* 2016 5: e14315.
39. Anenberg E, Chan AW, Xie Y, et al. Optogenetic stimulation of GABA neurons can decrease local neuronal activity while increasing cortical blood flow. *J Cereb Blood Flow Metab* 2015; 35: 1579–1586.
40. Dahlqvist MK, Thomsen KJ, Postnov DD, et al. Modification of oxygen consumption and blood flow in mouse somatosensory cortex by cell-type-specific neuronal activity. *J Cereb Blood Flow Metab*. Epub ahead of print 23 October 2019. DOI: 10.1177/0271678X19882787.
41. Vazquez AL, Fukuda M and Kim SG. Inhibitory neuron activity contributions to hemodynamic responses and metabolic load examined using an inhibitory Optogenetic Mouse Model. *Cereb Cortex* 2018; 28: 4105–4119.
42. Harris S, Ma H, Zhao M, et al. Coupling between gamma-band power and cerebral blood volume during recurrent acute neocortical seizures. *Neuroimage* 2014; 97: 62–70.
43. Berwick J, Johnston D, Jones M, et al. Fine detail of neurovascular coupling revealed by spatiotemporal analysis of the hemodynamic response to single whisker stimulation in rat barrel cortex. *J Neurophysiol* 2008; 99: 787–798.
44. Boorman L, Harris S, Bruyns-Haylett M, et al. Long-latency reductions in gamma power predict hemodynamic changes that underlie the negative BOLD signal. *J Neurosci* 2015; 35: 4641–4656.
45. Devor A, Tian P, Nishimura N, et al. Suppressed neuronal activity and concurrent arteriolar vasoconstriction may explain negative blood oxygenation level-dependent signal. *J Neurosci* 2007; 27: 4452–4459.
46. Han K, Min J, Lee M, et al. Neurovascular coupling under chronic stress is modified by altered GABAergic interneuron activity. *J Neurosci* 2019. DOI: 10.1523/JNEUROSCI.1357-19.2019.
47. Sceniak MP and Maciver MB. Cellular actions of urethane on rat visual cortical neurons in vitro. *J Neurophysiol* 2006; 95: 3865–3874.
48. Tuor UI and Farrar JK. Pial vessel caliber and cerebral blood flow during hemorrhage and hypercapnia in the rabbit. *Am J Physiol* 1984; 247: H40–H51.
49. Dimidschstein J, Chen Q, Tremblay R, et al. A viral strategy for targeting and manipulating interneurons across vertebrate species. *Nat Neurosci* 2016; 19: 1743–1749.
50. Yardeni T, Eckhaus M, Morris HD, et al. Retro-orbital injections in mice. *Lab Anim (NY)* 2011; 40: 155–160.
51. Dana H, Chen TW, Hu A, et al. Thy1-GCaMP6 transgenic mice for neuronal population imaging in vivo. *PLoS One* 2014; 9: e108697.
52. Chen TW, Wardill TJ, Sun Y, et al. Ultrasensitive fluorescent proteins for imaging neuronal activity. *Nature* 2013; 499: 295–300.

53. Tremblay R, Lee S and Rudy B. GABAergic interneurons in the Neocortex: from cellular properties to circuits. *Neuron* 2016; 91: 260–292.
54. Lee E, Lee J and Kim E. Excitation/inhibition imbalance in animal models of autism spectrum disorders. *Biol Psychiatry* 2017; 81: 838–847.
55. He HY and Cline HT. What is excitation/inhibition and how is it regulated? A case of the elephant and the Wisemen. *J Exp Neurosci* 2019; 13: 1179069519859371.
56. Dehghani N, Peyrache A, Telenczuk B, et al. Dynamic balance of excitation and inhibition in human and monkey Neocortex. *Sci Rep* 2016; 6: 23176.
57. Gu Y, Ge SY and Ruan DY. Effect of 4-aminopyridine on synaptic transmission in rat hippocampal slices. *Brain Res* 2004; 1006: 225–232.
58. Vilagi I, Dobo E, Borbely S, et al. Repeated 4-aminopyridine induced seizures diminish the efficacy of glutamatergic transmission in the neocortex. *Exp Neurol* 2009; 219: 136–145.
59. Avoli M, de Curtis M, Gnatkovsky V, et al. Specific imbalance of excitatory/inhibitory signaling establishes seizure onset pattern in temporal lobe epilepsy. *J Neurophysiol* 2016; 115: 3229–3237.
60. Ziburkus J, Cressman JR and Schiff SJ. Seizures as imbalanced up states: excitatory and inhibitory conductances during seizure-like events. *J Neurophysiol* 2013; 109: 1296–1306.
61. Buhl EH, Tamas G and Fisahn A. Cholinergic activation and tonic excitation induce persistent gamma oscillations in mouse somatosensory cortex in vitro. *J Physiol* 1998; 513: 117–126.
62. Levin AR and Nelson CA. Inhibition-based biomarkers for autism spectrum disorder. *Neurotherapeutics* 2015; 12: 546–552.
63. Buzsaki G and Wang XJ. Mechanisms of gamma oscillations. *Annu Rev Neurosci* 2012; 35: 203–225.
64. Cardin JA, Carlen M, Meletis K, et al. Driving fast-spiking cells induces gamma rhythm and controls sensory responses. *Nature* 2009; 459: 663–667.
65. Sohal VS, Zhang F, Yizhar O, et al. Parvalbumin neurons and gamma rhythms enhance cortical circuit performance. *Nature* 2009; 459: 698–702.
66. Siegle JH, Pritchett DL and Moore CI. Gamma-range synchronization of fast-spiking interneurons can enhance detection of tactile stimuli. *Nat Neurosci* 2014; 17: 1371–1379.
67. Chen G, Zhang Y, Li X, et al. Distinct inhibitory circuits orchestrate cortical beta and gamma band oscillations. *Neuron* 2017; 96: 1403–1418.
68. Logothetis NK. What we can do and what we cannot do with fMRI. *Nature* 2008; 453: 869–878.
69. Mateo C, Knutsen PM, Tsai PS, et al. Entrainment of arteriole vasomotor fluctuations by neural activity is a basis of blood-oxygenation-level-dependent “resting-state” connectivity. *Neuron* 2017; 96: 936–948.
70. Shmuel A and Leopold DA. Neuronal correlates of spontaneous fluctuations in fMRI signals in monkey visual cortex: Implications for functional connectivity at rest. *Hum Brain Mapp* 2008; 29: 751–761.
71. Scholvinck ML, Maier A, Ye FQ, et al. Neural basis of global resting-state fMRI activity. *Proc Natl Acad Sci U S A* 2010; 107: 10238–10243.
72. Fergus A and Lee KS. GABAergic regulation of cerebral microvascular tone in the rat. *J Cereb Blood Flow Metab* 1997; 17: 992–1003.
73. Kocharyan A, Fernandes P, Tong XK, et al. Specific subtypes of cortical GABA interneurons contribute to the neurovascular coupling response to basal forebrain stimulation. *J Cereb Blood Flow Metab* 2008; 28: 221–231.
74. McCormick DA and Contreras D. On the cellular and network bases of epileptic seizures. *Annu Rev Physiol* 2001; 63: 815–846.
75. Lacroix A, Toussay X, Anenberg E, et al. COX-2-derived prostaglandin E2 produced by pyramidal neurons contributes to neurovascular coupling in the rodent cerebral cortex. *J Neurosci* 2015; 35: 11791–11810.
76. Lecrux C, Toussay X, Kocharyan A, et al. Pyramidal neurons are “neurogenic hubs” in the neurovascular coupling response to whisker stimulation. *J Neurosci* 2011; 31: 9836–9847.
77. Trevelyan AJ, Sussillo D and Yuste R. Feedforward inhibition contributes to the control of epileptiform propagation speed. *J Neurosci* 2007; 27: 3383–3387.
78. Trevelyan AJ and Schevon CA. How inhibition influences seizure propagation. *Neuropharmacology* 2013; 69: 45–54.
79. Kepecs A and Fishell G. Interneuron cell types are fit to function. *Nature* 2014; 505: 318–326.
80. Markram H, Toledo-Rodriguez M, Wang Y, et al. Interneurons of the neocortical inhibitory system. *Nat Rev Neurosci* 2004; 5: 793–807.
81. Shiri Z, Levesque M, Etter G, et al. Optogenetic low-frequency stimulation of specific neuronal populations abates ictogenesis. *J Neurosci* 2017; 37: 2999–3008.
82. Krook-Magnuson E, Armstrong C, Oijala M, et al. On-demand optogenetic control of spontaneous seizures in temporal lobe epilepsy. *Nat Commun* 2013; 4: 1376.
83. Assaf F and Schiller Y. The antiepileptic and ictogenic effects of optogenetic neurostimulation of PV-expressing interneurons. *J Neurophysiol* 2016; 116: 1694–1704.
84. Maheshwari A, Marks RL, Yu KM, et al. Shift in interictal relative gamma power as a novel biomarker for drug response in two mouse models of absence epilepsy. *Epilepsia* 2016; 57: 79–88.
85. Selten M, van Bokhoven H and Nadif Kasri N. Inhibitory control of the excitatory/inhibitory balance in psychiatric disorders. *F1000Res* 2018; 7: 23.
86. Xue M, Atallah BV and Scanziani M. Equalizing excitation-inhibition ratios across visual cortical neurons. *Nature* 2014; 511: 596–600.
87. Urban A, Rancillac A, Martinez L, et al. Deciphering the neuronal circuitry controlling local blood flow in the cerebral cortex with optogenetics in PV::Cre transgenic mice. *Front Pharmacol* 2012; 3: 105.
88. Guillon B, Duncan R, Biraben A, et al. Correlation between interictal regional cerebral blood flow and



- depth-recorded interictal spiking in temporal lobe epilepsy. *Epilepsia* 1998; 39: 67–76.
89. Boscolo Galazzo I, Mattoli MV, Pizzini FB, et al. Cerebral metabolism and perfusion in MR-negative individuals with refractory focal epilepsy assessed by simultaneous acquisition of (18)F-FDG PET and arterial spin labeling. *Neuroimage Clin* 2016; 11: 648–657.
  90. Farrell JS, Gaxiola-Valdez I, Wolff MD, et al. Postictal behavioural impairments are due to a severe prolonged hypoperfusion/hypoxia event that is COX-2 dependent. *Elife* 2016; 5: e19352.
  91. Arango-Lievano M, Boussadia B, De Terdonck LDT, et al. Topographic reorganization of cerebrovascular mural cells under seizure conditions. *Cell Rep* 2018; 23: 1045–1059.
  92. Leal-Campanario R, Alarcon-Martinez L, Rieiro H, et al. Abnormal capillary vasodynamics contribute to ictal neurodegeneration in epilepsy. *Sci Rep* 2017; 7: 43276.
  93. Devinsky O. Therapy for neurobehavioral disorders in epilepsy. *Epilepsia* 2004; 45: 34–40.
  94. Salami P, Levesque M, Gotman J, et al. Distinct EEG seizure patterns reflect different seizure generation mechanisms. *J Neurophysiol* 2015; 113: 2840–2844.
  95. Reddy DS. Neurosteroids: endogenous role in the human brain and therapeutic potentials. *Prog Brain Res* 2010; 186: 113–137.
  96. Reddy DS. Role of hormones and neurosteroids in epileptogenesis. *Front Cell Neurosci* 2013; 7: 115.
  97. Tauboll E, Sveberg L and Svalheim S. Interactions between hormones and epilepsy. *Seizure* 2015; 28: 3–11.
  98. Lambert JJ, Belelli D, Peden DR, et al. Neurosteroid modulation of GABAA receptors. *Prog Neurobiol* 2003; 71: 67–80.
  99. Hosie AM, Wilkins ME, da Silva HM, et al. Endogenous neurosteroids regulate GABAA receptors through two discrete transmembrane sites. *Nature* 2006; 444: 486–489.
  100. Verrotti A, Latini G, Manco R, et al. Influence of sex hormones on brain excitability and epilepsy. *J Endocrinol Invest* 2007; 30: 797–803.
  101. Martin C, Zheng Y, Sibson NR, et al. Complex spatio-temporal haemodynamic response following sensory stimulation in the awake rat. *Neuroimage* 2013; 66: 1–8.
  102. Gao YR, Ma Y, Zhang Q, et al. Time to wake up: Studying neurovascular coupling and brain-wide circuit function in the un-anesthetized animal. *Neuroimage* 2017; 153: 382–398.